1 **Tradeoff Between Speed and Robustness in Primordium Initiation Mediated by**

2 **Auxin-CUC1 Interaction**

3

4 Shuyao Kong,[1,2] Mingyuan Zhu,[1,2,3] David Pan,[1,2] Brendan Lane,[4] Richard S. Smith,[4] Adrienne H.

5 K. Roeder[1,2,5,*]

6

7 [1] Weill Institute for Cell and Molecular Biology, Cornell University, Ithaca, NY 14853, USA

8 [2] Section of Plant Biology, School of Integrative Plant Science, Cornell University, Ithaca, NY

9 14853, USA

10 [3] Present address: Department of Biology, Duke University, Durham, NC 27708, USA

11 [4] Department of Computational and Systems Biology, John Innes Centre, Norwich NR4 7UH, UK.

12 [5] Lead Contact

13 [*] Correspondence: ahr75@cornell.edu

14 ABSTRACT

15 Robustness is the reproducible development of a phenotype despite stochastic noise. It often

16 involves tradeoffs with other performance metrics, but the mechanisms underlying such tradeoffs

17 were largely unknown. An *Arabidopsis* flower robustly develops four sepals from four precisely

18 positioned auxin maxima. The *development related myb-like 1* (*drmy1)* mutant generates

19 stochastic noise in auxin signaling that disrupts both the robust position and number of sepal

20 primordia. Here, we found that increased expression of *CUP-SHAPED COTYLEDON1* (*CUC1*),

21 a boundary specification transcription factor, in the *drmy1* mutant underlies this loss of

22 robustness. CUC1 surrounds and amplifies stochastic auxin patches in *drmy1* to form variably

23 positioned auxin maxima and sepal primordia. Removing *CUC1* from *drmy1* provides time for the

24 noise in auxin signaling to resolve into four precisely positioned auxin maxima, restoring robust

25 sepal initiation. However, removing CUC1 decreases auxin maxima intensity and slows down

26 sepal initiation. Thus, CUC1 increases morphogenesis speed but impairs robustness against

27 auxin noise. Further, using a computational model, we found that the observed phenotype can be

28 explained by the effect of CUC1 in repolarizing PIN FORMED1 (PIN1), a polar auxin transporter.

29 Thus, our study illustrates a tradeoff between speed and robustness during development.

30

31 **Keywords:** Robustness, tradeoff, primordium initiation, sepal, Arabidopsis, auxin, CUC1

32

33 **INTRODUCTION**

34   Cells within an organism experience a multitude of noise, such as stochastic gene

35   expression[1] and heterogenous growth rate[2,3]. Despite such noise, organisms often develop

36   invariantly and reproducibly, a phenomenon termed developmental robustness[4]. How

37   developmental robustness is achieved is one of the most intriguing open questions in cell biology[5],

38   which has attracted increasing research efforts in recent years[2,3,6–18]. It was shown that noise in

39   morphogen signaling can be buffered by certain gene regulatory network structures[13,14] and self-

40   organized cell sorting[11,15] to achieve robust patterning. Noise in growth rate can be buffered by

41   averaging growth among neighboring cells[2,3] or in the same cell over time[2] to achieve robust

42   organ size and shape. Notably, robustness is often involved in tradeoffs with other important

43   aspects of development[19–21]. For example, during porcine embryogenesis, manual removal of

44   zona pellucida speeds up development by a few hours but significantly reduces the robustness

45   of blastocysts development in terms of symmetry and cell size uniformity[21]. How such tradeoffs

46   are mediated remains largely unknown.

47   In plants, developmental robustness has been studied in sepals[2,3,16–18,22]. Sepals are the

48   outermost floral organs that enclose and protect the immature bud before the flower opens. To

49   achieve this protection, each flower robustly develops four sepals of constant size, positioned

50   evenly around the bud typical of a cruciferous flower. This robustness in size, number, and

51   position ensures tight closure critical for protection (Fig. 1a). In contrast, the *development related*

52   *myb-like 1* (*drmy1*) mutant produces 3-5 sepals of different sizes, unevenly positioned, leaving

53   gaps that expose the inner floral organs (Fig. 1a)[16,17]. This loss of developmental robustness

54   originates during the initiation of sepals from the floral meristem, where the sepal primordia are

55   robust in size, number, and position in wild type (WT) but variable in *drmy1* (Fig. 1b)[16]. We have

56   been studying how DRMY1 maintains robust sepal development. We previously showed that

57   DRMY1 maintains robustness by increasing TARGET OF RAPAMYCIN (TOR) signaling and

58   protein translation, which supports the rapid synthesis of A-type ARABIDOPSIS RESPONSE

59   REGULATOR (ARR) proteins to dampen cytokinin signaling. A proper level of cytokinin signaling

60   ensures robust patterning of auxin signaling and sepal initiation. In *drmy1*, lack of A-type ARR

61   proteins and the consequent upregulation of cytokinin signaling increases stochastic noise in

62   auxin patterning, underlying variable sepal initiation[17]. However, whether there are any tradeoffs

63   between robustness and other properties of development in this system remains unknown.

64   Here, we found that a tradeoff exists between robustness and speed of sepal initiation

65   from the floral meristem. In WT, strong, robust auxin maxima restricts the expression of *CUP-*

66   *SHAPED COTYLEDON1* (*CUC1*), encoding a boundary-specifying transcription factor[23,24], to

67   precise boundary domains immediately outside the auxin maxima. CUC1 increases the intensity

68   of auxin maxima it surrounds, and promotes rapid sepal initiation. In *drmy1*, lack of robustness in

69   auxin patterning causes an expansion of *CUC1* expression. CUC1 amplifies stochastic auxin

70   noise in the *drmy1* floral meristem, forming variably positioned auxin maxima and sepal primordia.

71   Removing CUC1 slows down sepal initiation but provides robustness against noise. Thus, the

72   feedback interactions between auxin and CUC1 promotes rapid organogenesis under low noise

73   conditions, but disrupts robustness under high noise conditions. Our study thus illuminates the

74   mechanism behind the tradeoff between robustness and speed during organ initiation.

75

76   **RESULTS**

77   ***CUC1* is upregulated in *drmy1* mutant**

78   To gain insights into key mechanisms controlling developmental robustness, we

79   previously performed RNA-seq on inflorescence tissue of *drmy1* vs. WT at the stage of sepal

80   primordium initiation[17]. We found a 2.4-fold increase in the expression of *CUC1* in *drmy1*, but not

81   for its paralogs *CUC2* and *CUC3* (Fig. 1c). *CUC* genes encode NAC (NAM, ATAF1,2, CUC2)

82   family transcription factors important for boundary specification[23,24]. To investigate where *CUC1*

83   is upregulated within the floral meristem, we imaged the *CUC1* transcriptional reporter. In WT,

84   *CUC1* is expressed in four precisely specified boundaries separating the incipient sepal primordia

85   from the center of floral meristem and each other, first appearing in the lateral boundaries followed

86   by the outer and inner boundaries (Fig. 1d). In contrast, in *drmy1*, *CUC1* expression is expanded

87   and localized to the bud periphery in early stage 2 meristems (Fig. 1e, Supplementary Movie 1).

88   As the bud develops, this broadened expression coalesces into narrower, WT-like boundary

89   domains in some parts of the bud (Fig. 1e, arrowheads), but remains in the bud periphery in other

90   parts (Fig. 1e, brackets), correlated with the presence or absence of sepal outgrowth in stage 3.

91   *drmy1* shows a similar disruption in the protein accumulation pattern of CUC1 (Fig. 1f, g,

92   Supplementary Movie 2), as well as the expression and protein accumulation patterns of CUC2

93   (Supplementary Fig. 1).

94   It was previously shown that auxin inhibits the expression of *CUC* genes and restricts them

95   to organ boundaries[25–27]. In the WT floral meristem, CUC1 accumulates in four boundaries

96   immediately outside the four auxin maxima (Supplementary Fig. 2a). In *drmy1*, diffuse, bud

97   periphery-localized CUC1 colocalizes with diffuse, weak bands of auxin signaling. As these auxin

98   bands concentrate into variably positioned auxin maxima, CUC1 domains retreat from the bud

99   periphery and refine into boundaries around the auxin maxima (Supplementary Fig. 2b). These

100   observations led us to hypothesize that the broadened *CUC1* expression in *drmy1* is due to lack

101   of robust, concentrated auxin maxima. Consistent with this idea, buds treated with L-Kynurenine

102   (L-Kyn, inhibitor of auxin synthesis) or Naphthylphthalamic acid (NPA, inhibitor of polar auxin

103   transport), both of which reduce auxin maxima (Supplementary Fig. 2c, d), show an expansion of

104   *CUC1* expression into the bud periphery (Supplementary Fig. 2e, f). Treatment with both 1-

105   Naphthaleneacetic acid (NAA) and NPA, which uniformly increases auxin signaling around the

106   bud periphery (Supplementary Fig. 2d), largely represses *CUC1* expression, and only a weak ring

107   of *CUC1* expression immediately inside the bud periphery remains (Supplementary Fig. 2f).

108   These results support the idea that robust, concentrated auxin maxima are required for the

109   precise boundary expression of *CUC1*, and that *drmy1* shows expanded *CUC1* expression due

110   to diffuse auxin signaling.

111

CUC1 upregulation is necessary and sufficient for variable sepal initiation

113   We next tested the phenotypic consequence of _CUC1_ upregulation, by imaging plants in

114   which the repression of _CUC1_ by miR164[28–30] has been removed. Specifically, we imaged _miR164_

115   mutants (_eep1_[30], _mir164abc_[29]), and plants carrying _CUC1_ expression constructs in which the

116   miR164 target sequence has been mutated (_5mCUC1_[28] and _CUC1m-GFP_[30]). In WT, buds

117   robustly develop four sepal primordia that are evenly spaced (Fig. 1b, 2a)[16,17]. We found that this

118   robustness is disrupted in buds upregulating _CUC1_, which, similar to _drmy1_, produce a range of

119   2-6 sepal primordia that are unevenly spaced and of different sizes (Fig. 2b-e, Supplementary

120   Fig. 3a-h). In WT, uniform sepal size within each flower is achieved by coordinated initiation timing

121   between sepal primordia, where inner and lateral sepals initiate within 12 hours of the outer sepal

122   (Supplementary Fig. 4a, c)[16]. In contrast, in _drmy1_, variability of sepal size originates from the

123   disorganized initiation timing, where the initiation of the inner and lateral sepals are severely

124   delayed (Supplementary Fig. 4f, h)[16]. Similar to _drmy1_, we found that in buds upregulating _CUC1_,

125   the initiation of inner and lateral sepals are greatly delayed relative to the outer sepal, underlying

126   the variability in size (Supplementary Fig. 4a-c). In addition, the time difference between outer,

127   inner, and lateral sepal initiation events is more variable between buds (Supplementary Fig. 4c).

128   Overall, these results suggest that _CUC1_ overexpression is sufficient to disrupt the robustness in

129   number, position, and coordinated initiation timing of sepal primordia.

130   Our results show that _CUC1_ overexpression is sufficient for disrupting robustness in sepal

131   initiation, but is it also necessary? We found that the _drmy1 cuc1_ double mutant often robustly

132   develops four sepal primordia that are evenly spaced, rescuing the variability in sepal number

133   and position in _drmy1_ (Fig. 2f-k). The result is specific to _cuc1_ since the _drmy1 cuc2_ double mutant

134   exhibits disrupted robustness similar to _drmy1_ (Supplementary Fig. 3i-n). While the _cuc1_ mutation

135   restores robustness in sepal primordia number and position in _drmy1_, it does not restore

136   robustness in sepal primordia size and coordination of initiation timing (Supplementary Fig. 4d-

6

137   h), suggesting that other mechanisms also contribute to these defects. Overall, these results show

138   that *CUC1* upregulation causes the variability of sepal primordium number and position in *drmy1*.

139

140   **CUC1 increases auxin maxima intensity and facilitates rapid sepal initiation**

141   CUC1 functions redundantly with CUC2 and CUC3 in organ separation[31,32], and the *cuc1*

142   *cuc2* double mutant shows sepal fusion in stage 8 flowers[31]. However, *cuc1 cuc2* flowers robustly

143   initiate four sepal primordia at stage 4, suggesting that they are dispensable for sepal initiation.

144   Then why is *CUC1* still expressed so early on in the floral meristem, when it has the potential to

145   disrupt robustness when dysregulated (Fig. 2)? Comparing buds of similar size (as an indicator

146   of similar developmental progression), we found that overexpression of *CUC1* makes the outer

147   sepal primordium initiate earlier from the floral meristem (Fig. 3a-c). This increased speed in outer

148   sepal initiation correlated with an increase in auxin signaling (Fig. 4a, b). Mutation of *CUC1* delays

149   the initiation of all four sepals relative to bud size (Fig. 3d-f), correlated with weaker auxin signaling

150   maxima (Fig. 4a, b). These results suggest that CUC1 increases auxin maxima intensity, which

151   in turn promotes rapid sepal initiation to promptly cover and protect the developing floral meristem.

152   This beneficial role may explain why *CUC1* is expressed in the early-stage floral meristem despite

153   its potential in reducing developmental robustness when dysregulated, and suggests a potential

154   conflict between speed and robustness in sepal initiation.

155

156   **CUC1 amplifies sporadic auxin noise into variably positioned auxin maxima**

157   How does *CUC1* mislocalization disrupt developmental robustness in *drmy1*? There is

158   evidence that feedback interaction between CUC and auxin plays an important role in plant

159   morphogenesis[25], and we previously showed that the disrupted pattern of auxin signaling

160   underlies variable sepal initiation in *drmy1*[16]. Our results illustrated the first half of the feedback

161   loop where auxin regulates CUC1, by showing that diffuse auxin signaling underlies the

162   mislocalization of CUC1 expression in *drmy1* (Supplementary Fig. 2). Here, we hypothesized the

163   second half of the feedback loop where CUC1 regulates auxin, and tested whether CUC1

164   mislocalization disrupts robustness in auxin pattern in *drmy1*. In WT, four auxin maxima form

165   robustly, marking four incipient sepal primordia (Fig. 4a, Outer, Inner, Lateral, Lateral). We found

166   that this robustness is disrupted in *5mCUC1* (CUC1 overexpression), as additional auxin maxima

167   form (Fig. 4a, arrow). The *cuc1* single mutant forms four auxin maxima robustly, although weaker

168   (Fig. 4a, b). The *drmy1* single mutant, where CUC1 is upregulated and mislocalized, shows

169   diffuse, noisy bands of auxin signaling (Fig. 4a, brackets). Removing CUC1 from *drmy1* restores

170   four robustly positioned auxin maxima (Fig. 4a, c-d). Overall, these results are consistent with the

171   second half of the feedback loop where CUC1 mislocalization disrupts robustness in auxin

172   pattern.

173   How is robust auxin pattern disrupted when *CUC1* is upregulated, and restored when

174   *CUC1* is removed? To address this question, we live imaged buds of WT, *5mCUC1*, *cuc1*, *drmy1*,

175   and *drmy1 cuc1* every 6 hours from late stage 1 to early stage 3 (Fig. 4e-n). Initially, WT buds

176   show three robustly positioned auxin maxima. One of them is in the cryptic bract (a suppressed

177   inflorescence leaf), a remnant of floral meristem initiation[33–36]. The other two auxin maxima appear

178   in the incipient lateral sepals. These auxin maxima are later followed by two more in the incipient

179   outer and inner sepals (Fig. 4e, j, Supplementary Movie 3). In *5mCUC1*, some buds initially form

180   WT-like pattern of four auxin maxima, followed by additional ones in between (Fig. 4f, k, arrows,

181   Supplementary Movie 4). Other buds display more dynamic spatiotemporal changes in auxin

182   maxima localization (Supplementary Fig. 5). This suggests that *CUC1* overexpression disrupts

183   auxin patterning by inducing the formation of new auxin maxima and making them more dynamic.

184   In *cuc1*, auxin maxima sequentially and robustly form like in WT, although weaker (Fig. 4g, l,

185   Supplementary Movie 5). In *drmy1*, auxin signaling initially appears as diffuse, noisy bands with

186   sporadic patches of cells having stronger signal than neighboring cells which fluctuates over time

187   (Fig. 4h, m, brackets). These sporadic patches seed the subsequent formation of variably sized

188   and positioned auxin maxima (Fig. 4h, m, arrowheads). As the bud further expands, additional

189   auxin maxima form, similar to *5mCUC1* (Fig. 4h, m, arrows, Supplementary Movie 6). In *drmy1*

190   *cuc1*, auxin signaling initially accumulates in sporadic patches, but unlike *drmy1*, they fade away,

191   allowing the subsequent formation of the robust auxin pattern (Fig. 4i, n, asterisk, Supplementary

192   Movie 7). Our results suggest that increased *CUC1* expression disrupts robust auxin patterning

193   in *drmy1* by amplifying sporadic auxin noise to form variably positioned auxin maxima.

194   We next tested whether CUC1 amplifies sporadic auxin noise from sources other than the

195   *drmy1* mutation. It was previously shown that exogenous cytokinin alters patterns of polar auxin

196   transport[37,38], causing sporadic patches of PIN convergence and auxin signaling[16]. We

197   hypothesized that the cytokinin induced sporadic patches of auxin signaling would not be

198   amplified in the *cuc1* mutant, and over-amplified in *CUC1* overexpression (*5mCUC1*) buds.

199   Indeed, WT buds treated with the synthetic cytokinin 6-Benzylaminopurine (BAP) amplifies

200   sporadic auxin patches to form variably positioned auxin maxima and sepal primordia (Fig. 5a, b,

201   g-k). While BAP induces sporadic auxin noise in early stage 2 buds of *cuc1*, it quickly fades away,

202   and most buds robustly form four sepal primordia (Fig. 5c, d, g-k). In contrast, *5mCUC1* buds

203   treated with BAP form numerous auxin maxima that often connect into a ring, which grow into 3-

204   8 primordia, more variable than the mock-treated, and often with mixed sepal-petal identity (Fig.

205   5e-k). Overall, these data support the idea that, under conditions that increase noise in auxin

206   patterning, such as *drmy1* or under exogenous cytokinin treatment, CUC1 amplifies the noise to

207   form variably positioned auxin maxima, which in turn disrupts robustness in sepal initiation. In the

208   absence of CUC1, these noisy patches are not amplified and quickly fade away, leaving four

209   robust auxin maxima.

210

211   **Modeling predicts CUC1 amplifies auxin noise by repolarizing PIN**

212   It was previously reported that *CUC* genes promote PIN polarity[25,39]. We wondered

213   whether an increase in PIN repolarization could explain the noise-amplifying effect of *CUC1*. To

214   test this, we implemented a computational model of auxin pattern formation (Supplementary

215   Dataset 2). The floral meristem was modeled using a 2D growing disk of cells, where cells divide

216   when a size threshold is met. In each cell, PIN1 transports auxin to neighboring cells with highest

217   auxin concentration. This up-the-gradient auxin transport has been shown to generate auxin

218   maxima patterns from a homogeneous initial condition with small perturbations[40–42] and is a

219   potential mechanism of auxin noise amplification. CUC1 is produced in cells with low auxin

220   concentration. The sole function of CUC1 in the model is to increase PIN repolarization. Below a

221   CUC1 concentration threshold, PIN repolarizes linearly according to the auxin concentration of

222   neighboring cells; above the threshold, PIN repolarizes quadratically, and is thus more sensitive

223   to auxin concentration differences among neighboring cells (Fig. 6a). We hypothesize that this

224   function of CUC1 in increasing PIN repolarization can by itself promote auxin maxima formation

225   while amplifying auxin noise. Starting with a patternless disk of cells with small fluctuations in

226   auxin production rate, auxin maxima form, which are then extracted and quantified (Fig. 6b). We

227   modeled the *drmy1* mutation by increasing the amplitude of fluctuation in auxin production rate,

228   which recreates the sporadic auxin patches and PIN convergence points observed in *drmy1*[16]

229   (Fig. 6c). We modeled the *cuc1* mutant by eliminating CUC1 production (Fig. 6c). We found that

230   in both WT and *drmy1* models, having CUC1 results in stronger, more concentrated auxin maxima

231   that form more rapidly compared to *cuc1* and *drmy1 cuc1* respectively (Fig. 6d-h). These modeling

232   results are similar to real buds (Fig. 4a, b). In both the model and the data, while *drmy1* amplifies

233   auxin production noise, creating variability in the final auxin pattern (Fig. 6f, arrowheads), *drmy1*

234   *cuc1* shows a relatively robust final pattern despite initial noise (Fig. 6g, arrows, 6i, Supplementary

235   Movie 8). These simulations suggest that the previously demonstrated function of CUC1 in

236   increasing PIN repolarization is sufficient for its role in promoting rapid, strong auxin maxima

237   formation while disrupting robustness against high auxin noise.

238   In addition to an increase in PIN repolarization which transports more auxin up the

239   concentration gradient, noise may also be amplified if a cell rapidly grows and divides, forming

240   two daughter cells that inherit the same auxin noise, before noise is dampened by transport or

241   decay (Supplementary Fig. 6a). To test this idea, we examined the effects of tissue growth rate

242   (which correlates with cell division rate in the model) on robustness of auxin patterning. We found

243   that increasing growth rate increases variability of auxin maxima in both WT and *drmy1*, while

244   reducing growth rate restores robust auxin patterning in *drmy1* (Supplementary Fig. 6b, d). In

245   *drmy1* simulations under reduced growth rate, the initial stochastic noise in auxin concentration

246   fades, allowing the formation of robust auxin pattern (Supplementary Fig. 6c), similar to

247   simulations of the *drmy1 cuc1* double mutant (Fig. 6g). This finding supports the idea that speed

248   and robustness can be conflicting sides of pattern formation during development.

249   It was previously shown that spatiotemporal averaging of cell heterogeneity can underlie

250   tissue-wide developmental robustness[2,43,44]. We hypothesize that reduced PIN sensitivity to

251   fluctuating auxin levels in neighboring cells (Fig. 6g) or reduced growth rate (Supplementary Fig.

252   6b, c) restores robust auxin patterning because they allow more time for auxin noise to average

253   to concentrations similar to nearby cells. We deduce that setting auxin noise temporally (but not

254   spatially) unchanging would eliminate this averaging (Supplementary Fig. 7a), and thus mutating

255   *cuc1* or reducing growth rate would no longer rescue the *drmy1* patterning defect. Indeed, when

256   noise is set temporally unchanging, both *drmy1* and *drmy1 cuc1* shows stabilization of initial auxin

257   noise into variably positioned auxin maxima, as does *drmy1* under reduced growth rate

258   (Supplementary Fig. 7b-d). Overall, these results support our idea that increased CUC1 disrupts

259   robustness in auxin patterning by increasing the sensitivity of PIN to fluctuating auxin levels, which

260   hinders temporal noise averaging and promotes noise amplification.

261

DISCUSSION

263   Developmental robustness has fascinated biologists for over 80 years[45], yet the underlying

264   mechanisms have just begun to be explored[2–4,6–18]. Here, we elucidated a mechanism through

265   which the developmental robustness of sepals is shaped by DRMY1-auxin-CUC1 interaction (Fig.

266   6j). In the floral meristem, DRMY1 maintains robust auxin patterning[16] which in turn restricts the

267   expression of *CUC1* to precise boundary domains adjacent to auxin maxima (Fig. 1d, f,

268   Supplementary Fig. 2). CUC1 increases the intensity of auxin maxima and promotes rapid sepal

269   initiation (Fig. 3, 4a, b). In the *drmy1* mutant, diffuse, noisy auxin signaling causes an upregulation

270   and expansion of the *CUC1* expression domain (Fig. 1e, g, Supplementary Fig. 2). CUC1

271   amplifies sporadic auxin patches to form variably positioned auxin maxima and sepal primordia

272   (Fig. 4, 5). In the *drmy1 cuc1* double mutant, auxin fluctuations have time to average out, allowing

273   robust auxin pattern formation (Fig. 6, Supplementary Fig. 7) and robust sepal initiation (Fig. 2).

274   In an Arabidopsis flower, sepals enclose and protect the inner, developing floral organs

275   before the flower opens. To achieve this function, they need to not only rapidly initiate from the

276   floral meristem to promptly cover it, but also develop robustly so as to not leave any gaps (Fig.

277   1a). We found that these two traits, speed and robustness, are conflicting sides of sepal

278   development, and that this tradeoff is mediated by auxin-CUC1 interaction. CUC1 promotes

279   strong auxin maxima formation and rapid sepal initiation, but also stabilizes auxin noise and can

280   therefore disrupt robustness under high auxin noise (Fig. 6j, left). On the other hand, lack of CUC1

281   slows down sepal development, but also allows time for noisy auxin signaling to robustly converge

282   (Fig. 6j, right).

283   Our computational modeling suggest that this speed-robustness tradeoff can be fully

284   explained by the previously reported function of CUCs in increasing PIN polarity[25,39]. How CUCs

285   increase PIN polarity remains unknown. It was shown that PIN polarity can be regulated by

286   phosphorylation (e.g., PID[46], D6PK[47], and PP2A[48]) or membrane trafficking (e.g., ABCB19[49] and

287   ROP2[50]). Thus, CUCs may increase PIN polarity by changing the expression of these important

288   PIN regulators. Alternatively, CUCs may also inhibit growth, causing mechanical conflict with

289   adjacent fast-growing regions which alters PIN polarity[51]. Further study is needed to test whether

290   CUCs increase PIN polarity by any of these mechanisms.

291   Is morphogenesis speed always involved in a tradeoff with robustness? Can a system

292   achieve both aspects simultaneously? Earlier theoretical studies on the mammalian olfactory

293   epithelium suggest that tissue regeneration regulated by a feedback loop cannot achieve both

294   speed and robustness, unless a second feedback loop is involved[19,20]. Similarly, a recent study

295   on Hedgehog signaling shows that coupled extracellular and intracellular feedback loops

296   mediated by PTCH provides both robustness and speed of signaling gradient formation,

297   compared to single or uncoupled feedback loops[13]. In summary, at the cost of additional

298   regulatory mechanisms, morphogenesis speed and robustness may be both achieved

299   simultaneously.

MATERIALS AND METHODS

Plant material

Most Arabidopsis plants were in Col-0 background (WT). Plants presented in Supplementary Fig. 1, 3a-c, 3e-f, and 7e were in Ler background. *mir164abc* was in a mixed Ler-Col background[29]. *drmy1* (Ler) was generated by backcrossing *drmy1* (Col-0) with Ler twice. The following lines were provided by the Arabidopsis Biological Resource Center: *pCUC2::3xVENUS-N7* (CS23891)[52], *pCUC2::CUC2-VENUS pPIN1::PIN1-GFP* (CS67929)[52], *pCUC1::CUC1m-GFP* (CS65830)[30], *cuc1-13* (SALK_006496C), *cuc2-3* (CS875298), *eep1* (CS65826)[30], and *mir164a-4 mir164b-1 mir164c-1* (CS65828)[29]. In addition, the following lines were previously described: *drmy1-2*[16], *5mCUC1*[28], *pCUC1::3xVENUS-N7*[29], *pCUC1::CUC1-GFP*[53], *DR5rev::3xVENUS-N7*[52], *DR5rev::ER-mRFP1.2*[54], *35S::mCitrine-RCI2A*[16]. *pCUC1::3xVENUS-N7* in Col-0 background (Fig. 1d-e) was generated by transforming Col-0 plants with the *pCUC1::3xVENUS-N7* construct.

Plant growth conditions

Seeds were sown in wetted Lambert LM-111 soil and stratified at 4°C for 3-5 days. Plants were grown under 16 h – 8 h light-dark cycles (fluorescent light, 100 µmol m^{-1} s^{-1}) at 22°C in a Percival walk-in growth chamber.

Flower staging

Flower buds were staged as previously described[55].

Confocal microscopy

Confocal imaging was done as previously described[16,17]. Briefly, inflorescences were cut and dissected with a Dumont tweezer (Electron Microscopy Sciences, style 5, no. 72701-D) down to stage 9, inserted upright into a small petri dish (VWR, 60 x 15 mm) containing inflorescence culture medium (1/2 MS, 1% (w/v) sucrose, 1x Gamborg vitamin mixture, 0.1% (v/v) plant

326 preservative mixture (Plant Cell Technology), 1% (w/v) agarose, pH 5.8), further dissected down

327 to stage 6 (for static imaging) or stage 2 (for live imaging), immersed with water, and imaged

328 under a Zeiss710 upright confocal microscope with a 20x Plan-Apochromat water-dipping lens

329 (1.0 NA). For static imaging, to visualize tissue morphology, samples were stained with 0.1 mg/ml

330 propidium iodide (PI) for 5 minutes before imaging. For live imaging, dissected samples were put

331 in a 24 h-light growth chamber (fluorescent light, 100 µmol $m^{-1}s^{-1}$) between time points. To prevent

332 bacterial growth, every 2-3 days, samples were transferred onto fresh media and treated with 100

333 µg/ml Carbenicillin (GoldBio, C-103-5, lot # 0129.091814A).

334   The following lasers and wavelengths were used. Chlorophyll, excitation 488 or 514 nm,

335 emission 660-722 nm (when also imaging mRFP1.2) or 647-721 nm (others). Propidium iodide,

336 excitation 514 nm, emission 590-660 nm. mRFP1.2, excitation 561 nm, emission 582-657 nm.

337 mCitrine, excitation 514 nm, emission 519-580 nm. For VENUS, in *DR5::3xVENUS-N7* and

338 *pCUC2::CUC2-VENUS*, excitation 514 nm, emission 519-558 nm; in *pCUC1::3xVENUS-N7*,

339 excitation 514 nm, emission 518-578 nm; in *pCUC2::3xVENUS-N7*, excitation 488 nm, emission

340 493-550 nm. GFP, excitation 488 nm, emission 493-556 nm.

341

342 **Image processing**

343   Image processing was done as previously described[16,17] and also briefly described below.

344   Tissue morphology was visualized by taking screenshots of the Chlorophyll, PI, or

345 *35S::mCitrine-RCI2A* channels in MorphoGraphX[56] or by 3D rendering in the ZEN software

346 (Processing → 3D). For Fig. 3 and Supplementary Fig. 4, to aid visualization of sepal initiation,

347 Gaussian curvature heatmaps were calculated in MorphoGraphX as follows: Gaussian blur (X/Y/Z

348 sigma = 1 µm twice and then X/Y/Z sigma = 2 µm once), edge detection (threshold = 2000-8000

349 depending on brightness, multiplier = 2.0, adapt factor = 0.3, fill value = 30000), marching cube

350 surface (cube size = 8 µm, threshold = 20000), change lookup table to "jet", subdivide mesh,

351 smooth mesh (passes = 5), subdivide mesh, smooth mesh (passes = 5), and project mesh

352   curvature (type = Gaussian, neighborhood = 10 µm, autoscale = no, min curv = -0.002, max curv

353   = 0.002). A sepal primordium is considered initiated when it emerges as a deep red band (positive

354   curvature) separated from the floral meristem by a deep blue band (negative curvature).

355   For circular histograms and kymographs of DR5 signal, each stack was cropped in ImageJ

356   and trimmed using the Voxel Edit function in MorphographX[56] so that only the focal bud remained

357   in the stack. The bud was positioned so that it was centered, facing the Z direction, and the

358   incipient outer sepal was at 45°. A circular histogram was calculated using the function Export

359   Histogram Circular, summing signal (in voxel intensity units, 0-255) in each 1° sector around the

360   Z axis starting from 0° (between the incipient outer and lateral sepals) counterclockwise. These

361   histograms were then 4°-binned and used for plotting mean ± SD and kymographs. Total signal

362   was calculated by summing all the bins.

363

364   **Quantification of developmental robustness**

365   For variability in sepal primordium position, within each bud, an angle was measured

366   between each pair of adjacent sepal primordia with respect to the bud center. CV was calculated

367   within each bud as a measurement of how evenly sepal primordia are distributed around the bud.

368   For relative initiation timing of sepals within each bud, we considered that the robust

369   temporal sepal initiation pattern in WT consists of the inner sepal initiating within 6 hours of the

370   outer sepal, and the lateral sepal initiating within 12 hours of the outer sepal[16]. Severely delated

371   inner and lateral sepal initiation indicate loss of robustness. Thus, for each genotype, we

372   calculated, among all buds, the mean and SD of initiation timing difference between inner and

373   outer sepals, and between lateral and outer sepals. Robustness is considered lost if sepal

374   initiation does not follow the WT temporal pattern (mean is greater than 6 and 12 respectively),

375   and also if different buds have different temporal patterns (SD is large).

376   For sepal initiation timing relative to bud size, bud area (μm^2) in maximum intensity

377   projection images were measured in ImageJ[57,58] and used as a proxy for bud size. Representative

378   images of WT vs. *cuc1* (both carrying 35S::mCitrine-RCI2A, a plasma membrane marker) that

379   are of similar area and growth rate throughout the time series were shown. Similarly for WT vs.

380   *5mCUC1*, although they did not have a membrane marker and thus the Chlorophyll channel was

381   used for area measurement. Bud size at the time of outer, inner, and lateral (WT vs *cuc1*) sepal

382   initiation was plotted. For *5mCUC1*, not enough samples initiated lateral sepals, and thus bud

383   size at the time of lateral sepal initiation was not analyzed. We reasoned that buds whose sepals

384   initiate rapidly should be smaller when they initiate sepals, compared to buds whose sepals take

385   longer to initiate. To control for the gradual reduction in size of successive buds during prolonged

386   *in vitro* culture, only buds that did not have any sepals at the first time point and produced at least

387   one sepal at or before the fourth time point (within 18 hours of the first time point) are analyzed.

388

389   ***In vitro* drug treatments on inflorescence samples**

390   For BAP treatment in Fig. 5, inflorescences were dissected, put onto an inflorescence

391   culture medium (see above) containing 0.05% DMSO and 1 µM BAP (6-Benzylaminopurine, Alfa

392   Aesar, A14678). Mock contained just 0.05% DMSO. They were left in a growth chamber for 32

393   hours and then transferred onto inflorescence culture medium without treatments, and imaged at

394   0 h, 24 h, 48 h, and 72 h after the transfer. For BAP treatment in Supplementary Fig. 7e,

395   inflorescences were cultured on media containing 0.01% DMSO and 5 µM BAP (mock contained

396   just 0.01% DMSO) for 96 h, and PI-stained and imaged.

397   For L-Kyn treatment, inflorescences were dissected and put onto an inflorescence culture

398   medium containing 0.02% DMSO and 80 µM L-Kyn (l-kynurenine, Sigma, K8625). Mock

399   contained just 0.02% DMSO. They were left in a growth chamber for 4 days before imaging.

400   For NPA and NPA+NAA treatment, inflorescences were dissected and put onto

401   inflorescence culture medium. The following solutions were made in water: for mock, 0.05%

402   DMSO, 0.01% Silwet L-77; for NPA, 100 µM NPA (Naptalam, Sigma, 33371), 0.05% DMSO,

403   0.01% Silwet L-77; for NPA+NAA, 100 µM NPA, 20 µM NAA (1-Naphthaleneacetic acid, Sigma,

404   N0640), 0.05% DMSO, 0.01% Silwet L-77. These solutions were applied on top of the dissected

405   inflorescences for 24 hours. Then, the solutions were discarded, and samples were washed three

406   times with sterile water. Images were taken 48 hours (for *DR5::3xVENUS-N7*) or 72 hours (for

407   *pCUC1::3xVENUS-N7*) after the end of the treatment.

408

409   **Mass-spring model of a growing floral meristem**

410   We modeled the stage 2 floral meristem as a 2D disk of growing and dividing cells. The

411   simulation begins as a round disk of 73 cells and 348 walls with no auxin, no CUC1, and apolar

412   PIN. As detailed below, in each iteration, the following processes are run in order: deformation of

413   cell walls under turgor pressure (repeated until convergence); dilution of auxin and CUC due to

414   changes in cell size; updating noise in auxin production; 10 steps of chemical interactions; cell

415   division; splitting of cell walls longer than 1 μm; cell growth; reinitialization; data output. The result

416   of each iteration was used as the starting point of the next. Simulations were run for the desired

417   number of iterations. Screenshots and data were saved every 10 iterations.

418   For tissue mechanics, a mass-spring model was used. Cell walls are subdivided to have

419   a maximum length of 1 μm. Wall segments are represented by springs in the simulation, with an

420   initial resting length the same as in the starting configuration. Uniform turgor pressure is simulated

421   by assigning a normal force to the boundary walls, as it cancels out on interior walls. The force

422   acting on a vertex v due to the springs was calculated as:

423    $$F_v = \sum_{n \in N_v} k \left(\frac{\|p_n - p_v\|}{L_{v:n}} - 1 \right) \frac{p_n - p_v}{\|p_n - p_v\|}$$

424   where N_v are neighboring vertices of vertex v, p_v is the position of vertex v, p_n is the position of a

425   neighboring vertex n, k is the spring constant (stiffness), and $L_{v:n}$ is the resting length of the spring

426   joining v and n[59,60]. Stiffness is set uniform and constant for all the cell walls. The resulting system

427   of equations is solved using the backward Euler method with the GPU based stabilized bi-

18

428   conjugate gradient solver available in MorphoDynamX. Growth was simulated by increasing the

429   rest length of the springs based on their relative stretch, multiplied by an extensibility factor g:

430
$$\frac{dL_{v:n}}{dt} = g\left(\frac{\|p_n - p_v\| - L_{v:n}}{L_{v:n}}\right)$$

431   Within each simulation, extensibility were set constant and uniform for all cell walls. Extensibility

432   was changed when modeling meristems with increased or decreased growth rate.

433   The molecular interactions are that (1) auxin represses CUC1 expression, and (2) CUC1

434   increases the sensitivity of PIN repolarization to auxin concentration differences among

435   neighboring cells. To simulate them, each cell is assigned two fields, auxin concentration (aux)

436   and CUC concentration (cuc). Each wall segment is assigned two fields, pin_P and pin_N, denoting

437   the amount of PIN protein on each side that mediates polar auxin transport in either direction. At

438   each chemical step, three calculations take place concomitantly:

439   (a) For each cell i at time step t, the amount of PIN on its wall facing neighboring cell j is

440   calculated as:

441
$$pin_{i \to j}(t) = (1 - \alpha)pin_{i \to j}(t - 1) + \alpha \frac{aux_j^n L_j}{\sum_{k \in N_i} aux_k^n L_k}$$

442
$$pin_{i \to j}(0) = \frac{L_j}{\sum_{k \in N_i} L_k}$$

443   where $\alpha = 0.01$ is the PIN repolarization speed, N_i is all the neighboring cells of cell i, L_j and L_k

444   are lengths of cell walls of cell i facing neighboring cells j and k respectively, and aux_j and aux_k

445   are the auxin concentrations of cell j and k respectively. n is the PIN sensitivity factor dependent

446   on the CUC concentration of cell i, cuc_i, and the threshold CUC concentration, $cuc_{thres} = 2$:

447
$$n = \begin{cases} 1 \ (cuc_i < cuc_{thres}) \\ 2 \ (cuc_i > cuc_{thres}) \end{cases}$$

448   Note that the total amount of PIN in each cell sums to 1 over all its cell walls, unaffected by auxin

449   concentration. Also note that a zero-flux boundary condition was used, i.e., no PIN is polarized

450   towards the boundary of the modeled tissue, and there is no flux of auxin across the boundary.

19

451   (b) Change in auxin concentration in cell i due to production, decay, and transport

452
$$\frac{d(aux_i)}{dt} = Prod_{aux} \times \delta_{aux,i} - Dec_{aux} \times aux_i + \frac{Tran_{aux} \sum_{j \in N_i}(aux_j \times pin_{j \to i} - aux_i \times pin_{i \to j})}{Area_i}$$

453   where $Prod_{aux} = 1$ is the auxin production coefficient, $Dec_{aux} = 0.2$ is the auxin decay coefficient,

454     $Tran_{aux} = 400$ is the polar auxin transport coefficient, N_i are the neighboring cells of i, $Area_i$ is

455   the area of cell i, $pin_{i \to j}$ is the amount of PIN on the wall of cell i facing neighbor j, and $pin_{j \to i}$ is

456   the amount of PIN on the wall of neighbor j facing cell i. $\delta_{aux,i}$ is the auxin production noise of cell

457   i, drawn during initialization and at each iteration from a Gaussian distribution $N(1, SD_{aux})$ where

458     $SD_{aux} = 0.1$ for WT and *cuc1*, and $SD_{aux} = 1$ for *drmy1* and *drmy1 cuc1*, and negative values are

459   set to 0. If the noise is set temporally unchanging (Supplementary Fig. 7), δ_{aux} values are drawn

460   only during initialization but not at each iteration.

461   (c) Change in CUC concentration in cell i due to production and decay

462
$$\frac{d(cuc_i)}{dt} = Prod_{cuc} \times \frac{1}{1 + (\frac{aux_i}{K_{aux}})^{hill}} - Dec_{cuc} \times cuc_i$$

463   where $Prod_{cuc}$ is the CUC production coefficient (1 for WT and *drmy1*, and 0 for *cuc1* and *drmy1*

464   *cuc1*), $Dec_{cuc} = 0.2$ is the CUC decay coefficient, $K_{aux} = 5$ is the concentration of auxin at which

465   CUC production is halved, and $hill = 4$ is an arbitrary Hill coefficient.

466   For cell division, a cell divides when its area passes a threshold of 50 μm^2. Position of the

467   new wall follows the minimal wall length principle, with noise parameters as follows (constant for

468   all simulations): cell division noise 2.0, cell center noise 2.0, wall junction noise 2.0. Daughter

469   cells inherit the same aux, cuc, and δ_{aux}. Split cell walls inherit pin_P and pin_N proportional to their

470   new lengths. New cell walls are assigned infinitesimal (non-zero) starting values of pin_P and pin_N.

471

472   **Software**

473   Image processing was done in ImageJ (version 2.14.0/1.54f, build c89e8500e4)[57,58] and

474   MorphoGraphX (version 2.0, revision 1-354, CUDA version 11.40)[56]. Modeling was implemented

475   in C++ using vlab (version 5.0, build #3609)[61] and MorphoDynamX (version 2.0, revision 2-1395,

476   CUDA version 11.40; www.MorphoDynamX.org) in an Ubuntu 20.04.6 LTS system, equipped with

477   an Intel Core i9-10900X 3.7 GHz 10-Core Processor, G.Skill Trident Z RGB 256 GB DDR4-3600

478   CL18 Memory, and a NVIDIA GeForce RTX 4090 24 GB Graphics Card. Data processing was

479   done in RStudio (R version 4.3.1 (2023-06-16) -- "Beagle Scouts")[62]. Graphs were made using

480   the package ggplot2 (version 3.4.2)[63]. Fisher's contingency table tests were done using

481   fisher.test. Wilcoxon rank sum tests were done using wilcox.test. Levene's tests of

482   homoscedasticity were done using leveneTest in package "car" (version 3.1-2). Data fitting with

483   ANOVA was done using the function aov. Figures were assembled in Adobe Illustrator (version

484   27.8.1). An RGB color profile "Image P3" was used for all the figures.

485

486   **Statistical analysis**

487   In most cases, each bud, either from the same inflorescence, a different inflorescence

488   from the same plant, or a different plant, is considered a biological replicate. For RNA-seq

489   presented in Fig. 1c, each RNA sample from 5-10 inflorescences of *ap1 cal AP1-GR* background

490   (either WT or *drmy1*), extracted separately, is considered a biological replicate.

491   For bar plots of sepal primordium number or auxin maxima number, all buds (or

492   simulations) were groups by genotype, and then grouped by number, and plotted as stacked bars.

493   For bar-and-whisker plots in Fig. 1c, 4b, 6h, Supplementary Fig. 4c, 4h, bar shows mean, and

494   whiskers show mean ± SD. For violin plots in Fig. 2e, 2k, Supplementary Fig. 3h, 3n, horizontal

495   lines show the quartiles. For circular histograms in Fig. 4d and 5g, lines show mean, and shaded

496   area shows mean ± SD.

497   Student's t-tests in Fig. 4b and Wilcoxon's rank sum tests in Fig. 2e, 2k, Supplementary

498   Fig. 3h, 3n, 4c, 4h are two-tailed, and compare only the indicated pairs of genotypes. For Levene's

499   test of variability in Supplementary Fig. 4c, 4h, center of each group were calculated as mean.

500   For ANOVA, formulae, degree of freedom, F, and p values are indicated in the Figure legends.

501   For Tukey's HSD in Fig. 6h, 6i, Supplementary Fig. 6d, 7d, all groups (combinations of genotype

502   and growth rate) were fit using a linear model, Estimated Marginal Means (EMM) were calculated,

503   and significant differences were indicated using compact letter display.

504   For RNA-seq, an FDR of 0.05 was used. For Tukey's HSD, family-wise type I error rate

505   was 0.05. For all other analyses, a p-value threshold of 0.05 was used.

506

507   **Data availability**

508   Data behind all the graph quantifications are available in Supplementary Dataset 1. RNA

509   seq data are available in GEO under project number PRJNA957462 and dataset number

510   GSE230100.

511

512   **Code availability**

513   Source code for the computational model, a tutorial, and demo data are available in

514   Supplementary Dataset 2 and also on GitHub (https://github.com/RoederLab/MassSpringAuxin).

515

516 **REFERENCES**

517   1.   Araújo, I. S. *et al.* Stochastic gene expression in *Arabidopsis thaliana*. *Nat. Commun.* **8**,

518   2132 (2017).

519   2.   Hong, L. *et al.* Variable Cell Growth Yields Reproducible Organ Development through

520   Spatiotemporal Averaging. *Dev. Cell* **38**, 15–32 (2016).

521   3.   Le Gloanec, C. *et al.* Cell type-specific dynamics underlie cellular growth variability in

522   plants. *Dev.* **149**, dev200783 (2022).

523   4.   Lachowiec, J., Queitsch, C. & Kliebenstein, D. J. Molecular mechanisms governing

524   differential robustness of development and environmental responses in plants. *Ann. Bot.*

525   **117**, 795–809 (2016).

526   5.   Roeder, A. H. K. *et al.* Fifteen compelling open questions in plant cell biology. *Plant Cell*

527   **34**, 72–102 (2022).

528   6.   Hintze, M., Katsanos, D., Shahrezaei, V. & Barkoulas, M. Phenotypic Robustness of

529   Epidermal Stem Cell Number in *C. elegans* Is Modulated by the Activity of the Conserved

530   N-acetyltransferase nath-10/NAT10. *Front. Cell Dev. Biol.* **9**, 640856 (2021).

531   7.   Garelli, A., Gontijo, A. M., Miguela, V., Caparros, E. & Dominguez, M. Imaginal discs

532   secrete insulin-like peptide 8 to mediate plasticity of growth and maturation. *Science* **336**,

533   579–582 (2012).

534   8.   Folta, A. *et al.* Over-expression of Arabidopsis AtCHR23 chromatin remodeling ATPase

535   results in increased variability of growth and gene expression. *BMC Plant Biol.* **14**, 76

536   (2014).

537   9.   Cassidy, J. J. *et al.* MiR-9a minimizes the phenotypic impact of genomic diversity by

538   buffering a transcription factor. *Cell* **155**, 1556–1567 (2013).

539   10.   Maugarny, A. *et al.* Compensation of compromised PRC2 regulation by a miRNA ensures

540   robustness of Arabidopsis leaf development. *Preprint at bioRxiv:*

541   https://doi.org/10.1101/2023.10.11.561475 (2023).

542   11.   Tsai, T. Y. C. *et al.* An adhesion code ensures robust pattern formation during tissue
543   morphogenesis. *Science* **370**, 113–116 (2020).

544   12.   Besnard, F. *et al.* Cytokinin signalling inhibitory fields provide robustness to phyllotaxis.
545   *Nature* **505**, 417–421 (2014).

546   13.   Li, P. *et al.* Morphogen gradient reconstitution reveals Hedgehog pathway design
547   principles. *Science* **360**, 543–548 (2018).

548   14.   Winter, K. U. *et al.* Evolution of class B floral homeotic proteins: Obligate heterodimerization
549   originated from homodimerization. *Mol. Biol. Evol.* **19**, 587–596 (2002).

550   15.   Xiong, F. *et al.* Specified neural progenitors sort to form sharp domains after noisy Shh
551   signaling. *Cell* **153**, 550–561 (2013).

552   16.   Zhu, M. *et al.* Robust organ size requires robust timing of initiation orchestrated by focused
553   auxin and cytokinin signalling. *Nat. Plants* **6**, 686–698 (2020).

554   17.   Kong, S. *et al.* DRMY1 promotes robust morphogenesis by sustaining translation of a
555   hormone signaling protein. *Preprint at bioRxiv:* https://doi.org/10.1101/2023.10.11.561475
556   (2023).

557   18.   Trinh, D.-C. Increased gene expression variability hinders the formation of regional
558   mechanical conflicts leading to reduced organ shape robustness. *Proc. Natl. Acad. Sci.*
559   **120**, 2017 (2023).

560   19.   Lander, A. D., Gokoffski, K. K., Wan, F. Y. M., Nie, Q. & Calof, A. L. Cell lineages and the
561   logic of proliferative control. *PLoS Biol.* **7**, e1000015 (2009).

562   20.   Lander, A. D. Pattern, growth, and control. *Cell* **144**, 955–969 (2011).

563   21.   Li, R., Liu, Y., Pedersen, H. S., Kragh, P. M. & Callesen, H. Development and quality of
564   porcine parthenogenetically activated embryos after removal of zona pellucida.
565   *Theriogenology* **80**, 58–64 (2013).

566   22.   Roeder, A. H. K. Arabidopsis sepals: A model system for the emergent process of
567   morphogenesis. *Quant. Plant Biol.* **2**, e14 (2021).

568 23. Olsen, A. N., Ernst, H. A., Leggio, L. Lo & Skriver, K. NAC transcription factors: Structurally
569   distinct, functionally diverse. *Trends Plant Sci.* **10**, 79–87 (2005).

570 24. Aida, M. & Tasaka, M. Genetic control of shoot organ boundaries. *Curr. Opin. Plant Biol.*
571   **9**, 72–77 (2006).

572 25. Bilsborough, G. D. *et al.* Model for the regulation of *Arabidopsis thaliana* leaf margin
573   development. *Proc. Natl. Acad. Sci. U. S. A.* **108**, 3424–3429 (2011).

574 26. Furutani, M. *et al.* PIN-FORMED1 and PINOID regulate boundary formation and cotyledon
575   development in Arabidopsis embryogenesis. *Development* **131**, 5021–5030 (2004).

576 27. Aida, M., Vernoux, T., Furutani, M., Traas, J. & Tasaka, M. Roles of PIN-FORMED1 and
577   MONOPTEROS in pattern formation of the apical region of the Arabidopsis embryo.
578   *Development* **129**, 3965–3974 (2002).

579 28. Mallory, A. C., Dugas, D. V., Bartel, D. P. & Bartel, B. MicroRNA regulation of NAC-domain
580   targets is required for proper formation and separation of adjacent embryonic, vegetative,
581   and floral organs. *Curr. Biol.* **14**, 1035–1046 (2004).

582 29. Sieber, P., Wellmer, F., Gheyselinck, J., Riechmann, J. L. & Meyerowitz, E. M. Redundancy
583   and specialization among plant microRNAs: Role of the MIR164 family in developmental
584   robustness. *Development* **134**, 1051–1060 (2007).

585 30. Baker, C. C., Sieber, P., Wellmer, F. & Meyerowitz, E. M. The early extra petals1 mutant
586   uncovers a role for microRNA miR164c in regulating petal number in Arabidopsis. *Curr.*
587   *Biol.* **15**, 303–315 (2005).

588 31. Aida, M., Ishida, T., Fukaki, H., Fujisawa, H. & Tasaka, M. Genes involved in organ
589   separation in Arabidopsis: An analysis of the *cup-shaped cotyledon* mutant. *Plant Cell* **9**,
590   841–857 (1997).

591 32. Hibara, K. I. *et al.* Arabidopsis CUP-SHAPED COTYLEDON3 regulates postembryonic
592   shoot meristem and organ boundary formation. *Plant Cell* **18**, 2946–2957 (2006).

593 33. Dinneny, J. R., Yadegari, R., Fischer, R. L., Yanofsky, M. F. & Weigel, D. The role of

594   JAGGED in shaping lateral organs. *Development* **131**, 1101–1110 (2004).

595   34.   Long, J. & Barton, M. K. Initiation of axillary and floral meristems in Arabidopsis. *Dev. Biol.*

596   **218**, 341–353 (2000).

597   35.   Peng, Z. *et al.* Differential growth dynamics control aerial organ geometry. *Curr. Biol.* **32**,

598   4854-4868.e5 (2022).

599   36.   Ohno, C. K., Reddy, G. V., Heisler, M. G. B. & Meyerowitz, E. M. The Arabidopsis *JAGGED*

600   gene encodes a zinc finger protein that promotes leaf tissue development. *Development*

601   **131**, 1111–1122 (2004).

602   37.   Růžička, K. *et al.* Cytokinin regulates root meristem activity via modulation of the polar

603   auxin transport. *Proc. Natl. Acad. Sci. U. S. A.* **106**, 4284–4289 (2009).

604   38.   Marhavý, P. *et al.* Cytokinin controls polarity of PIN1-dependent Auxin transport during

605   lateral root organogenesis. *Curr. Biol.* **24**, 1031–1037 (2014).

606   39.   Galbiati, F. *et al.* An integrative model of the control of ovule primordia formation. *Plant J.*

607   **76**, 446–455 (2013).

608   40.   Reinhardt, D. *et al.* Regulation of phyllotaxis by polar auxin transport. *Nature* **426**, 255–260

609   (2003).

610   41.   Smith, R. S. *et al.* A plausible model of phyllotaxis. *Proc. Natl. Acad. Sci. U. S. A.* **103**,

611   1301–1306 (2006).

612   42.   Jönsson, H., Heisler, M. G., Shapiro, B. E., Meyerowitz, E. M. & Mjolsness, E. An auxin-

613   driven polarized transport model for phyllotaxis. *Proc. Natl. Acad. Sci. U. S. A.* **103**, 1633–

614   1638 (2006).

615   43.   Gregor, T., Tank, D. W., Wieschaus, E. F. & Bialek, W. Probing the Limits to Positional

616   Information. *Cell* **130**, 153–164 (2007).

617   44.   Erdmann, T., Howard, M. & Ten Wolde, P. R. Role of spatial averaging in the precision of

618   gene expression patterns. *Phys. Rev. Lett.* **103**, 2–5 (2009).

619   45.   Waddington, C. H. Canalization of Development and the Inheritance of Acquired

620   Characters. *Nature* **150**, 563–656 (1942).

621 46. Friml, J. *et al.* A PINOID-dependent binary switch in apical-basal PIN polar targeting directs

622   auxin efflux. *Science* **306**, 862–865 (2004).

623 47. Zourelidou, M. *et al.* Auxin efflux by PIN-FORMED proteins is activated by two different

624   protein kinases, D6 PROTEIN KINASE and PINOID. *eLife* **3**, e02860 (2014).

625 48. Michniewicz, M. *et al.* Antagonistic Regulation of PIN Phosphorylation by PP2A and

626   PINOID Directs Auxin Flux. *Cell* **130**, 1044–1056 (2007).

627 49. Titapiwatanakun, B. *et al.* ABCB19/PGP19 stabilises PIN1 in membrane microdomains in

628   Arabidopsis. *Plant J.* **57**, 27–44 (2009).

629 50. Nagawa, S. *et al.* ROP GTPase-dependent actin microfilaments promote PIN1 polarization

630   by localized inhibition of clathrin-dependent endocytosis. *PLoS Biol.* **10**, e1001299 (2012).

631 51. Heisler, M. G. *et al.* Alignment between PIN1 polarity and microtubule orientation in the

632   shoot apical meristem reveals a tight coupling between morphogenesis and auxin

633   transport. *PLoS Biol.* **8**, e1000516 (2010).

634 52. Heisler, M. G. *et al.* Patterns of auxin transport and gene expression during primordium

635   development revealed by live imaging of the Arabidopsis inflorescence meristem. *Curr.*

636   *Biol.* **15**, 1899–1911 (2005).

637 53. Gonçalves, B. *et al.* A conserved role for *CUP-SHAPED COTYLEDON* genes during ovule

638   development. *Plant J.* **83**, 732–742 (2015).

639 54. Marin, E. *et al.* mir390, Arabidopsis TAS3 tasiRNAs, and their AUXIN RESPONSE

640   FACTOR targets define an autoregulatory network quantitatively regulating lateral root

641   growth. *Plant Cell* **22**, 1104–1117 (2010).

642 55. Smyth, D. R., Bowman, J. L. & Meyerowitz, E. M. Early flower development in Arabidopsis.

643   *Plant Cell* **2**, 755–767 (1990).

644 56. Strauss, S. *et al.* Using positional information to provide context for biological image

645   analysis with MorphoGraphX 2.0. *eLife* **11**, e72601 (2022).

646   57.   Schindelin, J. *et al.* Fiji: An open-source platform for biological-image analysis. *Nat.*
647   *Methods* **9**, 676–682 (2012).

648   58.   Schindelin, J., Rueden, C. T., Hiner, M. C. & Eliceiri, K. W. The ImageJ ecosystem: An
649   open platform for biomedical image analysis. *Mol. Reprod. Dev.* **82**, 518–529 (2015).

650   59.   Majda, M. *et al.* Elongation of wood fibers combines features of diffuse and tip growth. *New*
651   *Phytol.* **232**, 673–691 (2021).

652   60.   Mosca, G. *et al.* Modeling Plant Tissue Growth and Cell Division. in *Mathematical Modelling*
653   *in Plant Biology* 107–138 (2018). doi:10.1007/978-3-319-99070-5_7.

654   61.   Federl & Prusinkiewicz. Virtual laboratory: an interactive software environment for
655   computer graphics. in *1999 Proceedings Computer Graphics International* 93–100 (1999).
656   doi:10.1109/CGI.1999.777921.

657   62.   R Core Team (2021). R: A language and environment for statistical computing. R
658   Foundation for Statistical Computing, Vienna, Austria. URL https://www.R-project.org/.

659   63.   Wickham, H. *ggplot2: Elegant Graphics for Data Analysis*. (Springer, 2009).
660   doi:10.1007/978-0-387-98141-3.

661

ACKNOWLEDGEMENTS

AUTHOR CONTRIBUTIONS

Conceptualization and design of experiments were done by S.K., M.Z., and A.H.K.R. Experiments were carried out by S.K. Data analysis was done by S.K. and D.P. The MorphoDynamX modeling platform was developed by B.L. and R.S.S. The floral meristem model was developed by S.K. based on scripts written by B.L. and R.S.S. Manuscript was prepared by S.K. and edited by all the authors. Funds were provided by A.H.K.R. and R.S.

COMPETING INTERESTS

The authors declare no competing interests.

MATERIALS AND CORRESPONDENCE

Material requests and correspondence should be addressed to A.H.K.R.

688   **FIGURES**
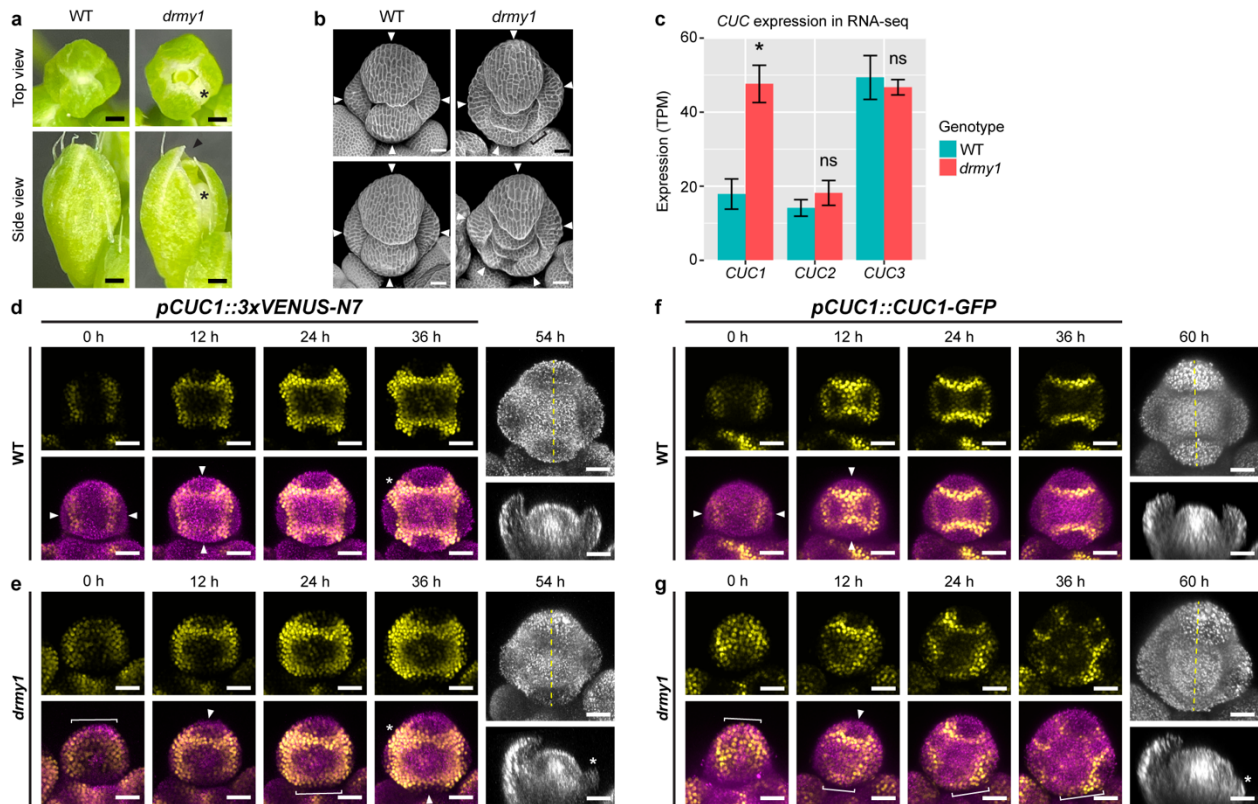
689

690   **Fig. 1. CUC1 is upregulated in *drmy1* with disrupted spatial pattern.**

691   **(a-b)** Floral phenotype of the *drmy1* mutant. **(a)** Stage 12 buds of WT (left) and *drmy1* (right). In

692   *drmy1*, asterisk indicates a gap on the side due to uneven sepal positions; arrowhead indicates a

693   gap on the top caused by unequal sepal length. Scale bars, 250 μm. **(b)** Two stage 6 buds of WT

694   (left), and two *drmy1* buds with matching outer sepal size. Arrowheads point to sepal primordia.

695   Note that sepal primordia in *drmy1* are of variable size, number, and position, leaving regions in

696   the bud periphery with no sepal outgrowth (bracket). Scale bars, 25 μm.

697   **(c)** Expression of *CUC* genes in floral tissue of WT vs *drmy1* (in Ler *ap1 cal AP1-GR* background),

698   as determined by RNA-seq. n = 3 samples per genotype. Adjusted p-values from DESeq2: CUC1,

699   3.710×10^{-13}; CUC2, 0.6650; CUC3, 0.2292. Complete dataset is in Kong et al. (2023)[17].

700   **(d-e)** Expression pattern of *CUC1* in WT **(d)** and *drmy1* **(e)**, live imaged through time. For 0 to 36

701   hours, top row shows *pCUC1::3xVENUS-N7*, and bottom row shows *pCUC1::3xVENUS-N7*

702   (yellow) merged with Chlorophyll (magenta; to show flower morphology). For 54 hours, the

703   chlorophyll channel and its longitudinal section (dashed lines) are shown. Note that in WT, four

704   boundaries with high *CUC1* expression form at robust positions between the incipient sepal

705   primordia and the center of the floral meristem at stage 2 (arrowheads), corresponding to the

706   robust initiation of four sepals at stage 3. In *drmy1*, *CUC1* expression expands to the bud

707   periphery (brackets). Although this peripheral expression later narrows to boundary domains

708   (arrowheads), it correlates with limited sepal outgrowth at stage 3 (asterisk). *CUC1* expression in

709   the inter-sepal regions are also expanded in *drmy1* (asterisks). See Supplementary Movie 1.

710   Images are representative of n = 4 WT buds and n = 5 *drmy1* buds. Note that plants are

711   heterozygous for *pCUC1::3xVENUS-N7*. Scale bars, 25 µm.

712   **(f-g)** Protein accumulation pattern of CUC1 in WT **(f)** and *drmy1* **(g)**, live imaged through time.

713   For 0 to 36 hours, top row shows *pCUC1::CUC1-GFP*, and bottom row shows *pCUC1::CUC1-*

714   *GFP* (yellow) merged with Chlorophyll (magenta). For 60 hours, the chlorophyll channel and its

715   longitudinal section (dashed lines) are shown. Note that in WT, four boundaries with high CUC1

716   protein accumulation form at robust positions between the incipient primordia and the center of

717   the floral meristem at stage 2 (arrowheads), corresponding to the robust initiation of four sepals

718   at stage 3. In *drmy1*, CUC1 protein accumulation is initially much higher and less boundary-

719   restricted, and often in the bud periphery (brackets). In some regions, CUC1 accumulation

720   narrows to boundary domains (arrowheads), while in other regions, it remains in the bud

721   periphery, correlated with limited sepal outgrowth at stage 3 (asterisk). See Supplementary Movie

722   2. Images are representative of n = 2 WT buds and n = 4 *drmy1* buds. Scale bars, 25 µm.

723

724

725
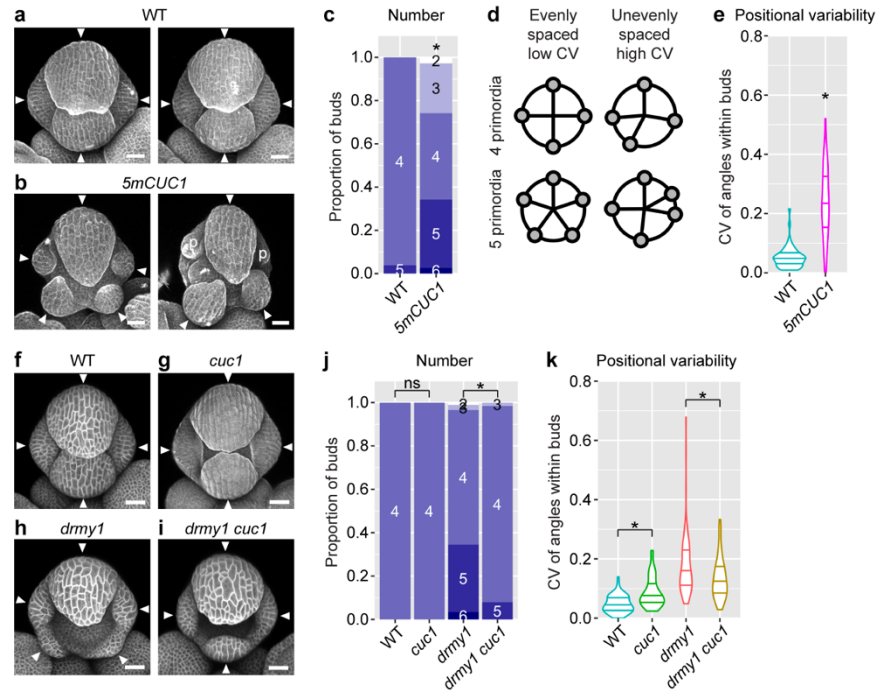
Fig. 2. *CUC1* upregulation is sufficient and necessary for variable sepal initiation

(a-e) *CUC1* upregulation causes variable sepal initiation. **(a-b)** Two representative WT **(a)** and *5mCUC1* **(b)** buds stained with PI. Arrowheads show sepal primordia. "p" shows petal primordia. Scale bars, 25 μm. **(c)** Quantification of sepal primordium number in each bud, color-coded by number and grouped by genotype. **(d)** Illustration of quantifying variability in sepal position. Buds in which sepal primordia are evenly distributed around the bud have low CV values of angular distanced between adjacent sepal primordia (left). Buds in which sepal primordia are irregularly positioned have high CV values of angles between adjacent sepals (right). Reproduced from Kong et al. (2023)[17]. **(e)** Quantification of positional variability in WT vs *5mCUC1*. Sample size: WT, n = 51 buds; *5mCUC1*, n = 70 buds. Asterisks indicate statistically significant differences from WT in a Fisher's contingency table test ($p = 4.535×10^{-14}$) **(c)** or Wilcoxon rank sum test ($p = 2.878×10^{-16}$) **(e)**.

(f-k) The *cuc1* mutation rescues variability in sepal number and position in *drmy1*. **(f-i)** Representative buds of WT **(f)**, *cuc1* **(g)**, *drmy1* **(h)**, and *drmy1 cuc1* **(i)**. The *cuc1* bud was PI-

740   stained, and others carried the *35S::mCitrine-RCI2A* membrane marker. Arrowheads point to

741   sepal primordia. Scale bars, 25 μm. **(j-k)** Quantification of sepal primordium number **(j)** and

742   positional variability **(k)** as described above. Sample size: WT, n = 66 buds; *cuc1*, n = 52 buds;

743   *drmy1*, n = 87 buds; *drmy1 cuc1*, n = 63 buds. Asterisks indicate statistically significant differences

744   in a Fisher's contingency table test **(j)** or Wilcoxon rank sum test **(k)**, and ns means no significant

745   differences. P-values for **(j)**: WT vs. *cuc1*, p = 1; *drmy1* vs. *drmy1 cuc1*, p = 2.575×10^{-4}. P-values

746   for **(k)**: WT vs. *cuc1*, p = 2.665×10^{-6}; *drmy1* vs. *drmy1 cuc1*, p = 4.922×10^{-3}.

Speed vs. Robustness in Primordium Initiation
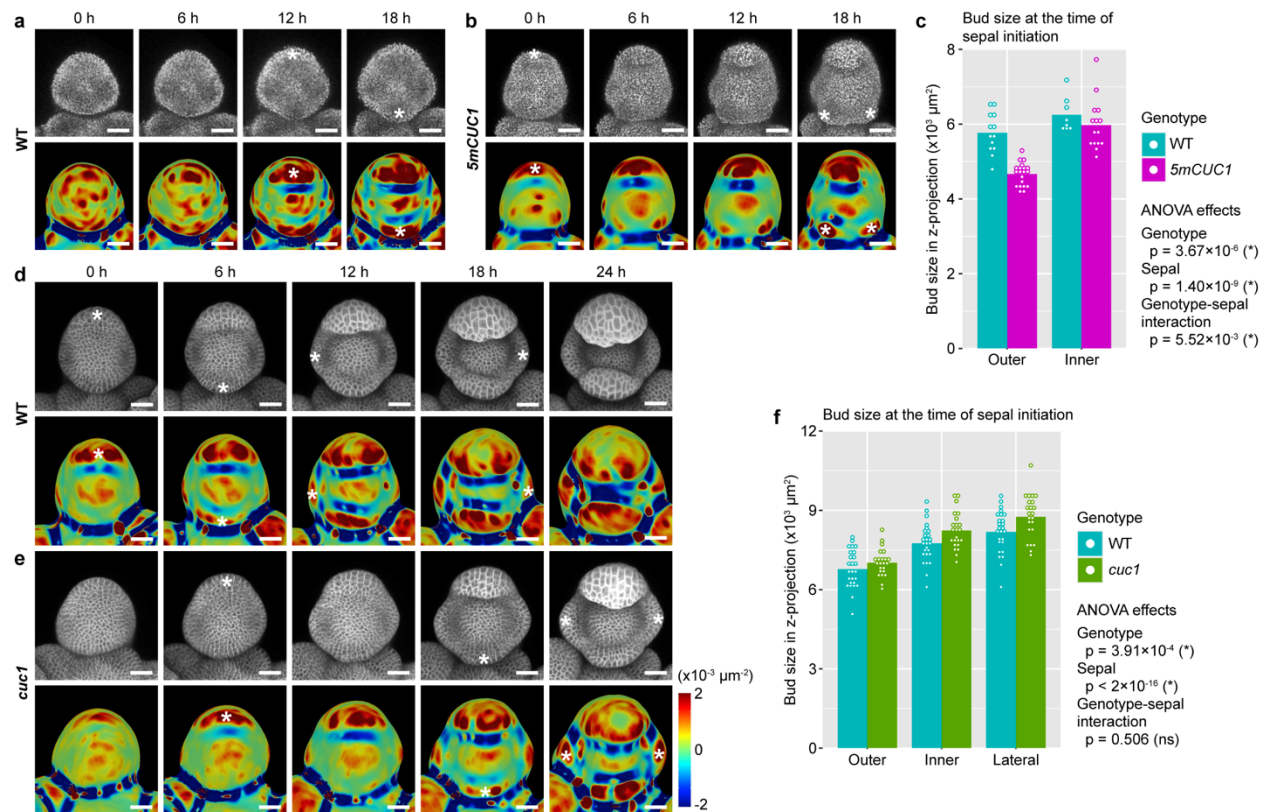
**Fig. 3. CUC1 promotes rapid sepal initiation.**

(a-c) The outer sepal initiates more rapidly in *5mCUC1* than WT. **(a,b)** show one bud of WT **(a)** and one bud of *5mCUC1* **(b)** live imaged every 6 hours for 18 hours. Chlorophyll channel is shown on the top, and Gaussian curvature of extracted surfaces is on the bottom. The buds were matched for size, indicating matched developmental stage. Asterisks indicate sepal initiation events. Note that outer sepal initiation was much earlier in *5mCUC1* than WT. **(c)** Quantification of bud size (area in Z-projections; as a proxy for developmental stage) at the time of sepal initiation. Shown are mean (bars) and individual buds (dots). Sample size, WT outer sepal, n = 13; *5mCUC1* outer sepal, n = 20; WT inner sepal, n = 8; *5mCUC1* inner sepal, n = 15. An ANOVA model of Size ~ Genotype * Sepal was fit. Genotype, degree of freedom (df) = 1, F = 26.823, p = 3.67×10^{-6}. Sepal, df = 1, F = 53.946, p = 1.40×10^{-9}. Interaction, df = 1, F = 8.387, p = 5.52×10^{-3}.

(d-f) Sepals initiate more slowly in *cuc1* than WT. **(d,e)** show one bud of WT **(d)** and one bud of *cuc1* **(e)** live imaged every 6 hours for 24 hours. Chlorophyll is shown on the top, and Gaussian

761   curvature of extracted surfaces is on the bottom. The buds were matched for size, indicating

762   matched developmental stage. Asterisks indicate sepal initiation events. Note that overall sepal

763   initiation is delayed in *cuc1* compared to WT. **(f)** Quantification of bud size (area in Z-projections;

764   as a proxy for developmental stage) at the time of sepal initiation. Shown are mean (bars) and

765   individual buds (dots). Sample size, 26 buds for WT and 23 buds for *cuc1*. An ANOVA model of

766   Size ~ Genotype * Sepal was fit. Genotype, df = 1, F = 13.198, p = 3.91×10^{-4}. Sepal, df = 2, F =

767   60.760, p < 2×10^{-16}. Interaction, df = 2, F = 0.685, p = 0.5055. Scale bar in all images, 25 μm.
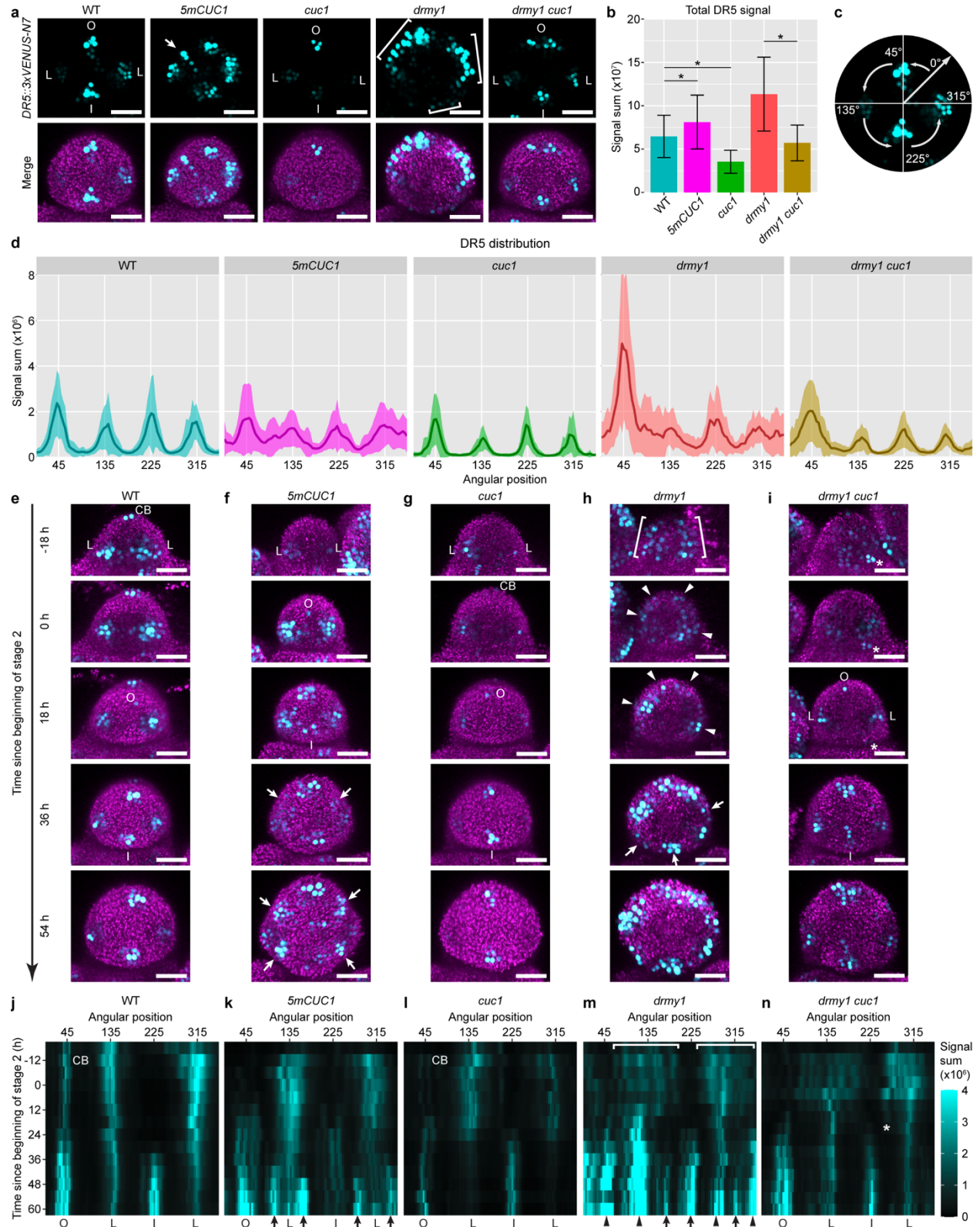
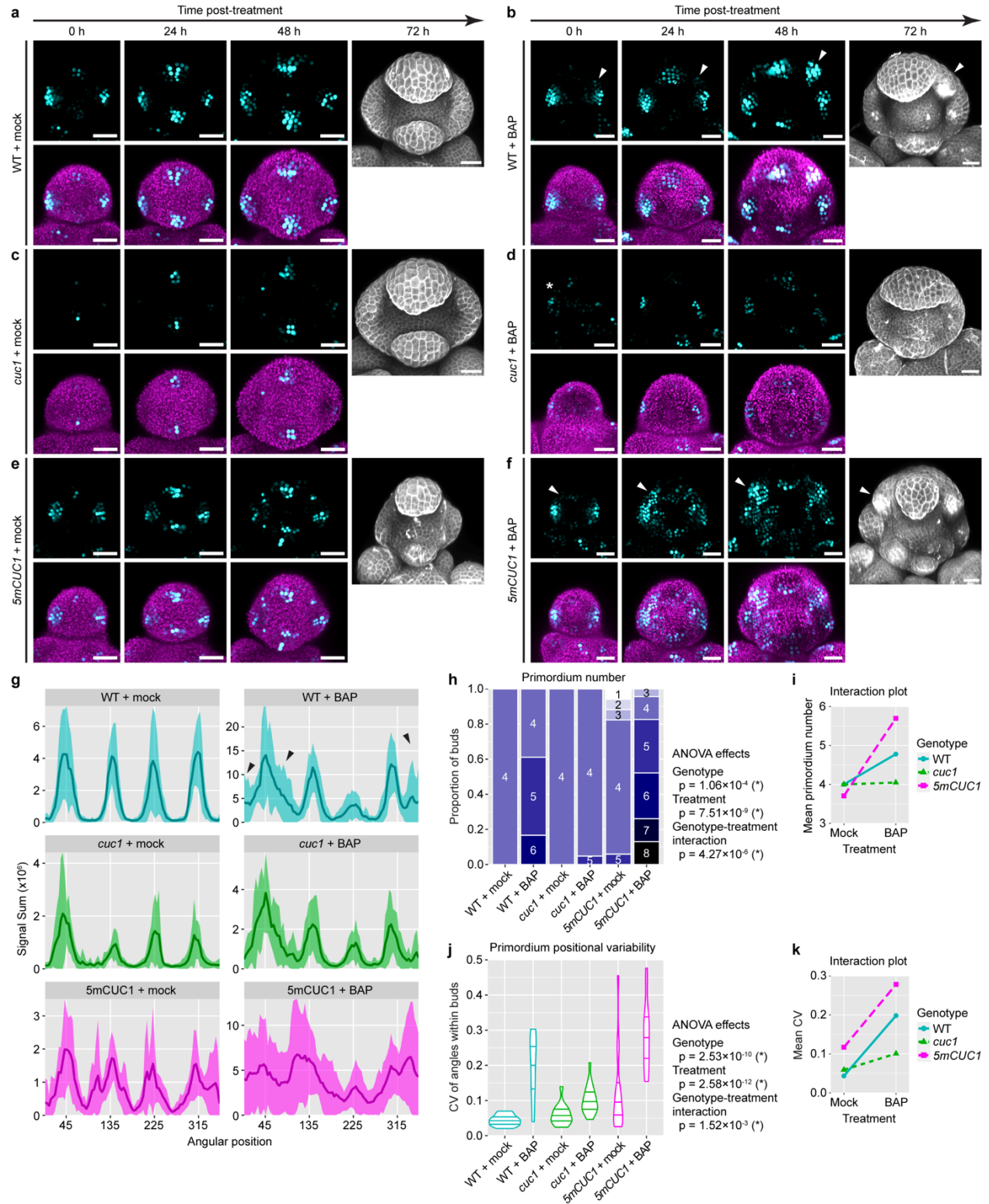Speed vs. Robustness in Primordium Initiation

768

36

769 **Fig. 4. CUC1 overexpression is necessary and sufficient for variability in auxin maxima**

770 **patterning**

771 **(a-d)** Auxin patterning is disrupted in *5mCUC1* and *drmy1* but rescued in *drmy1 cuc1*. **(a)**

772 Representative images of *DR5::3xVENUS-N7* (cyan, top row) and DR5 merged with the

773 chlorophyll channel (magenta, bottom row) in stage 2 buds of WT, *5mCUC1*, *cuc1*, *drmy1*, and

774 *drmy1 cuc1*. **(b)** Quantification of total DR5 signal (mean ± SD). Asterisks indicate statistically

775 significant differences in two-tailed t-tests (WT vs. *5mCUC1*, p = 0.0266; WT vs. *cuc1*, p =

776 2.09×10^{-6}; *drmy1* vs. *drmy1 cuc1*, p = 1.32×10^{-6}). **(c)** Illustration of circular histogram analysis in

777 **(d)** and **(j-n)**. Each bud was aligned so that the incipient outer sepal was on the top and the

778 inflorescence meristem on the bottom. DR5 signal was quantified in 4°-bins around the Z-axis

779 starting between the incipient lateral and outer sepal, so that the incipient outer sepal would be at

780 45°. **(d)** Circular histograms of DR5 in each genotype showing mean ± SD. Sample size: WT, n =

781 30 buds; *5mCUC1*, n = 29 buds; *cuc1*, n = 19 buds; *drmy1*, n = 24 buds; *drmy1 cuc1*, n = 32 buds.

782 **(e-n)** *CUC1* upregulation promotes auxin maxima formation, but can amplify sporadic auxin

783 patches. **(e-i)** Live imaging of stage 2 buds of WT, *5mCUC1*, *cuc1*, *drmy1*, and *drmy1 cuc1*

784 carrying *DR5::3xVENUS-N7*. Shown is DR5 (cyan) merged with the chlorophyll channel

785 (magenta). On the left shows time relative to the beginning of stage 2 (second row), an indicator

786 of developmental progression. **(j-n)** Kymographs showing DR5 signal through time, in the same

787 buds as in **(e-i)**. O, incipient outer sepal; I, incipient inner sepal; L, incipient lateral sepal; CB,

788 cryptic bract. Brackets indicate diffuse bands of auxin signaling that later form distinct, variably

789 positioned auxin maxima (arrowheads). Arrows indicate additional auxin maxima that form in the

790 space between existing ones. Asterisks indicate a sporadic auxin patch that gradually disappears

791 in *drmy1 cuc1*. Scale bar in all images, 25 µm.

792

793

Speed vs. Robustness in Primordium Initiation

Fig. 5. CUC1 amplifies sporadic auxin patches to form variably positioned auxin maxima and primordia.

38

797 **(a-f)** WT **(a,b)**, *cuc1* **(c,d)**, and *5mCUC1* **(e,f)** were treated with mock (DMSO) **(a,c,e)** or 1 µM

798 BAP **(b,d,f)** for 32 hours and then transferred onto non-treatment media (0 h) and live-imaged

799 every 24 hours for four time points. For 0 h, 24 h, and 48 h, top rows show *DR5::3xVENUS-N7*

800 (cyan) and bottom rows show DR5 merged with the Chlorophyll channel (magenta). For 72 h,

801 buds were PI-stained. Note that BAP treatment disrupts robust auxin patterning and causes

802 sporadic auxin patches. In *cuc1*, sporadic patches disappear (asterisk), whereas in WT and

803 *5mCUC1*, they are amplified to form variably positioned auxin maxima and sepal primordia

804 (arrowheads). Scale bars, 25 µm.

805 **(g)** Circular histograms of DR5 in late stage 2 and early stage 3 buds at 48 h post-treatment.

806 Shown is mean ± SD. Note that BAP treatment causes regions of great variability in WT (large

807 SD, black arrows), which is less pronounced in *cuc1* and more pronounced in *5mCUC1*. Sample

808 size: WT + mock, n = 11 buds; WT + BAP, n = 17 buds; *cuc1* + mock, n = 11 buds; *cuc1* + BAP,

809 n = 19 buds; *5mCUC1* + mock, n = 13 buds; *5mCUC1* + BAP, n = 20 buds.

810 **(h-k)** Quantification of variability in primordium number **(h,i)** and position **(j,k)** in stage 3 and 4

811 buds at 72 h post-treatment. **(h)** shows the number of primordia in each bud, grouped by

812 genotype. An ANOVA model of Number ~ Genotype * Treatment was fit. Genotype, df = 2, F =

813 10.04, p = 1.06×10^{-4}. Treatment, df = 1, F = 39.81, p = 7.51×10^{-9}. Interaction, df = 2, F = 14.01, p

814 = 4.27×10^{-6}. **(j)** shows a violin plot of the CV of angles between adjacent primordia in each bud.

815 An ANOVA model of CV ~ Genotype * Treatment was fit. Genotype, df = 2, F = 27.790, p =

816 2.53×10^{-10}. Treatment, df = 1, F = 63.585, p = 2.58×10^{-12}. Interaction, df = 2, F = 6.932, p =

817 1.52×10^{-3}. Note that both sepal and petal primordia were counted, as they were hard to distinguish

818 in many cases. **(i,k)** shows the respective interactions plots of mean primordium number **(i)** and

819 mean CV of position **(k)**. Note that *5mCUC1* further increases the variability caused by BAP

820 treatment, while *cuc1* is largely resistant to the effect of BAP. Sample size: WT + mock, n = 13

821 buds; WT + BAP, n = 18 buds; *cuc1* + mock, n = 15 buds; *cuc1* + BAP, n = 21 buds; *5mCUC1* +

822 mock, n = 17; *5mCUC1* + BAP, n = 23.

Speed vs. Robustness in Primordium Initiation

823
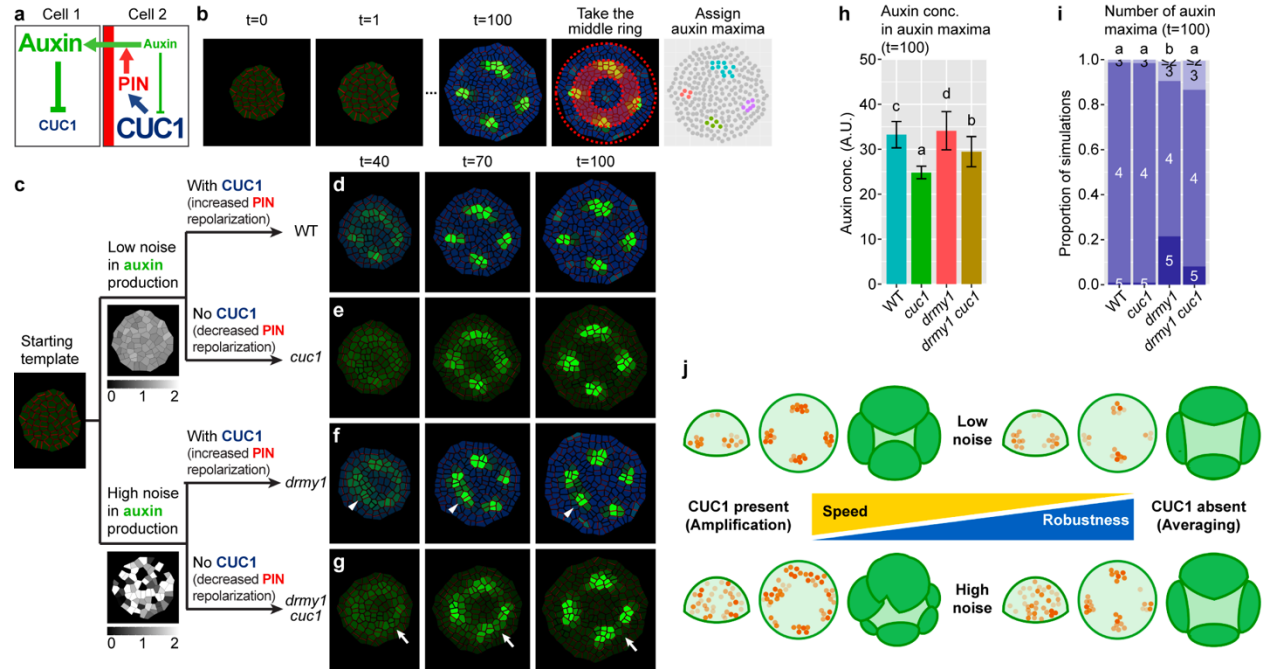
Fig. 6. The noise-amplifying effect of CUC1 can be fully explained by an increase in PIN repolarization.

(a) Diagram of auxin-CUC1 interaction implemented in the model. Auxin represses *CUC1* expression, whereas CUC1 increases PIN repolarization. PIN1 polarizes toward neighboring cells with highest auxin concentration and moves auxin out of the cell into its neighbors. **(b)** Modeling approach. The floral meristem is modeled with a 2D disk of cells, which starts patternless. Molecular interactions in **(a)** generate auxin distribution patterns. Auxin maxima within the shaded middle ring (1/3 < r < 2/3 of total radius) were extracted and quantified. **(c)** How genotypes were modeled. The *drmy1* mutation is modeled as having higher noise in auxin production. The *cuc1* mutation is modeled by removing CUC1 (which decreases PIN1 repolarization). **(d-i)** Removing CUC1 rescues the variability in auxin patterning of *drmy1*. Shown are simulations of WT **(d)**, *cuc1* **(e)**, *drmy1* **(f)**, and *drmy1 cuc1* **(g)**. Note that while a sporadic auxin patch in *drmy1* was amplified to form an auxin maximum (arrowhead), a similar patch in *drmy1 cuc1* dissipates (arrow). Growth rate, 0.8. **(h)** shows simulated auxin concentration averaged across all auxin maxima within each bud (mean ± SD). **(i)** shows the number of auxin maxima in each bud at t=100. Quantifications

40

839   were done across n=500 simulations of each genotype. Letters show multiple comparison using

840   Tukey's HSD. **(j)** A tradeoff exists between the speed and robustness of morphogenesis. Having

841   CUC1 promotes rapid morphogenesis under low noise conditions (top left), yet disrupts

842   robustness under high noise conditions such as *drmy1* or BAP treatment (bottom left). Removing

843   CUC1 reduces auxin maxima intensity and sepal initiation speed (top right), but allows additional

844   time for noise to dissipate and robust pattern to form under high noise conditions (bottom right).